Journal of Zhejiang University-SCIENCE A (Applied Physics & Engineering)
ISSN 1673-565X (Print); ISSN 1862-1775 (Online)
www.jzus.zju.edu.cn; www.springerlink.com
E-mail: jzus@zju.edu.cn

Evaluation of the oil/water selective plugging performance of nano-polymer microspheres in fractured carbonate reservoirs*

Jie WANG[1,2], Fu-jian ZHOU[†‡1,2], Jun-jian LI[1], Kai YANG[1,2], Lu-feng ZHANG[1,2], Fan FAN[1,2]

[1]*State Key Laboratory of Petroleum Resource and Prospecting, China University of Petroleum, Beijing 102249, China*

[2]*The Unconventional Natural Gas Institute, China University of Petroleum, Beijing 102249, China*

[†]E-mail: zhoufj@cup.edu.cn

Received June 12, 2019; Revision accepted Aug. 18, 2019; Crosschecked Aug. 22, 2019

Abstract: Water channeling of fractured carbonate rocks seriously restricts oil well production and is particularly prominent in the Troyes oilfield, located in the north of Kazakhstan. A nanometer particulate matter (PM) solution was used to evaluate the plugging ability of matrix and fractured core in a fractured carbonate model. Results showed that PM had good dispersion and swelling ability in simulated formation water. The swelling rate reached more than 300% in 3 d. PM had a perfect deep plugging effect in both matrix core and fractured core. The residual resistance coefficient of matrix and fractured core after plugging reached between 3.29 and 5.88, and the plugging rate was between 69.58% and 83.01%. The higher the residual resistance coefficient, the higher the plugging rate. PM has a good selective plugging effect on oil/water. The oil/water selection coefficient $R_{w/o}$ was less than 1.0 and close to 0, mainly because of the different mechanisms of oil/water and PM. Scanning electron microscope (SEM) imaging results showed that the plugging mechanism of PM in the throat and fractures was manifested mainly in three aspects: adsorptive retention, mechanical trapping, and agglomeration plugging. The mechanism was further verified by energy disperse spectroscopy (EDS) elemental analysis technology.

Key words: Nano-polymer microspheres; Fractured core; Plugging rate; Oil/Water selectivity; Plugging mechanism
https://doi.org/10.1631/jzus.A1900249 **CLC number:** TE34

1 Introduction

The development of natural fractures and the oil recovery rate of edge-bottom water reservoirs largely depend on the water-breakthrough time and water-flooding rate, which also restrict the production of oil reservoirs worldwide. The development and application of tertiary oil recovery technology has greatly mitigated the water-flooding problem (Yao et al., 2016). In particular, gel particle water shutoff technology has been widely used since its discovery (Bai et al., 2013). Recently, dispersed gel particles (Ranganathan et al., 1998), prefabricated gel particles (Wu and Bai, 2008), temperature-triggered microgels (Frampton et al., 2004), and pH-selective microgels (Al-Anazi and Sharma, 2002) have been widely used due to their small particle size, high swelling rate, and good dispersion (Rousseau et al., 2005; Al-Ibadi and Civan, 2012, 2013). However, gel particles are not applicable in the north Kazakhstan Troyes carbonate reservoir, due mainly to the size of the particles and a poor injection rate with micro fractures (fracture size

‡ Corresponding author

* Project supported by the Foundation of State Key Laboratory of Petroleum Resources and Prospecting, China University of Petroleum at Beijing (No. PRP/indep-4-1314), the Science Foundations of China University of Petroleum at Beijing (No. 462014YJRC015), and the National Science and Technology Major Project of China (No. 2015ZX05051003)

ORCID: Jie WANG, https://orcid.org/0000-0001-8279-741X; Fu-jian ZHOU, https://orcid.org/0000-0002-9050-3271

0.02–0.03 mm) and substrate cores (pore throat size 0.20–0.50 μm). Furthermore, a gel will plug the entrance and fail in effective sealing (Rousseau et al., 2005). Therefore, the gel particle size must be further reduced to match the fracture and throat size.

Zhao et al. (2019) synthesized an elastic particulate matter (PM) emulsion (median size 9.996 μm), evaluated the matching relationship between the pore throat and PM through core flow experiments in macro scale, and analyzed the PM plugging mechanism with scanning electron microscope (SEM) imaging. They believed that under an appropriate matching coefficient, a smaller-particle-size PM with high elastic modulus can show a strong sealing ability. Pu et al. (2018) used nuclear magnetic resonance (NMR) to test the oil/water distribution in cores after a micron-grade PM solution displacement experiment. Their visual microfluidic model revealed an oil increase mechanism of the PM solution. They believed the deformation produced by the migration of PM with high elasticity and low inflation had a better cleaning effect on residual oil in big holes. Micron-scale PM solution has good sealing performance, but there are injection issues for reservoirs with the same micron-scale throat. Dong et al. (2009) and Hua et al. (2014) prepared nano-agent microspheres (median particle size between 30 and 60 nm) using anti-microemulsion polymerization, and evaluated their basic physical properties. Nano-level PM can enter a smaller throat, penetrate deep into the reservoir, and form effective plugging. Microspheres enter the micro-pore throat to replace the crude oil in the channel, which increases oil production. Nanometer PM solution has good injectivity in micro fractures and small pores, and the oil displacement mechanism is known, but its plugging mechanism has not been well studied.

In this study of nanoscale PM solution, cores from a fractured carbonate reservoir in the north Kazakhstan Troyes oilfield, with a reservoir temperature of 54 °C and a natural fracture size of 0.02–0.03 mm, were chosen for model making. We comprehensively evaluated the sealing effect and oil/water selectivity of PM in carbonate matrix cores and fractured cores using a PM basic performance test, a core flow experiment, and micro methods of SEM or energy disperse spectroscopy (EDS). The results provide a reference for further applications in oilfields.

2 Experimental

2.1 Experimental material

Nano PM was provided by the Zhongke Polymerized Petroleum Technology Co., Ltd., Gansu, China. The main components were a dispersant and a polyacrylamide nano PM monomer. The salinity of simulated formation water from Troyes is 86 198 mg/L, with 30 000 mg/L Na^+ ions, 30 000 mg/L K^+ ions, 3006 mg/L Ca^{2+} ions, and 1000 mg/L Mg^{2+} ions. Other components included industrial kerosene and pure analytical grade ethanol. The lower Cretaceous natural carbonate core has a porosity between 16% and 25% and a permeability of 1.5–5.0 mD. To evaluate the sealing performance of microspheres at the core depth, the lengths of both fractured and matrix cores were greater than 30 cm.

After ethanol demulsification, repeated washing, and pure-air drying of the PM, the extracted samples were chosen for analysis of their structural characteristics using a VERTEX 70 Fourier transform infrared (FTIR) spectrometer and KBr tablet pressing method. The infrared spectrum of PM is shown in Fig. 1. The stretching vibration absorption peaks of C═O in the $–CONH_2$ group are shown at 1668 cm^{-1}, and primary amide N–H at 3194 cm^{-1} and 3357 cm^{-1}. The peaks at 2928 cm^{-1} and 2958 cm^{-1} correspond to C–H on saturated hydrocarbons CH_2 and CH. The bending vibration absorption peaks of C–H on saturated hydrocarbon CH_2 are at 1453 cm^{-1} and 1414 cm^{-1}. Therefore, we infer that the target product is polyacrylamide.

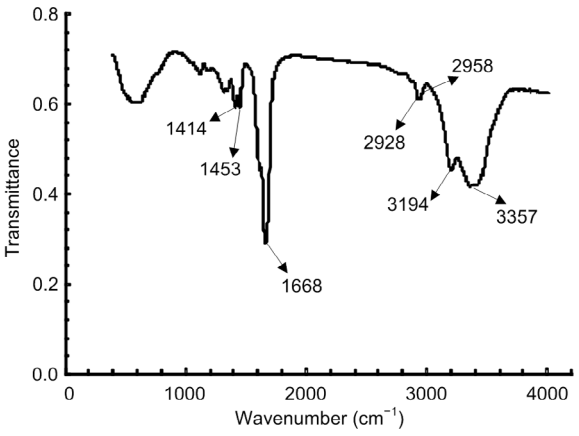

Fig. 1 PM FTIR spectrum

2.2 Experimental equipment

Laboratory equipment included a Zetasizer Nano (UK) laser nanometer particle size analyzer, in-house pressure multicore displacement device, and a Gemini SEM 300/VP (Germany) high resolution field emission SEM. Fig. 2 shows a flow chart of the experimental steps including the morphological study of dried hydration microspheres, hydration particle size test, sealing performance evaluation (including matrix cores and fractured cores), microsphere adsorption ability, and microcosmic research of the plugging mechanism of microspheres in the porous media.

2.3 Experimental procedure

2.3.1 Preparation of fractured core samples

In natural fractures developed in the Troyes reservoir, the fracture size is between 0.02 and 0.03 mm, and the permeability of the matrix fluid is 1–2 mD. To simulate the sealing effect of PM on fractured reservoirs, fractured carbonate rocks and fracture-free matrix carbonate rocks were selected for sealing experiments. The fractured carbonate samples were man-made in the laboratory as follows: (1) Cut matrix cores 30 cm long and 2.5 cm in diameter using a core cutter; (2) Split the cores using the Brazilian splitting method; (3) Paint a layer of honey uniformly on one side of the fracture to adhere to the proppant used to support the fracture (the honey was washed away with the fluid in the first stage of saturated saline solution, without affecting the fracture permeability); (4) Evenly spread a layer of 50 mesh proppant (size 0.300 mm) on the honey at a concentration of 4 kg/m^2; (5) Evenly spread a layer of honey on the other side of the fracture, merge the split core, fix the core with tape, and use it for the next experiment. The process of making cores of fractured carbonate rocks is shown in Fig. 3.

2.3.2 Equivalent width calculation of fractured cores

The equivalent width of simulated fractures under confining pressure was calculated to ensure the size of simulated fractures was consistent with that of natural fractures in actual reservoirs. According to Yang and Wei (2015), Eq. (1) for calculating the equivalent fracture width of the fracture-matrix system is as follows:

$$b=\sqrt[3]{3\pi d\left(K_{\mathrm{t}}-K_{\mathrm{m}}\right)}, \tag{1}$$

where b is the equivalent fracture width, cm; d is the core diameter, cm; K_{t} is the measured permeability of the fracture matrix system, cm^2; K_{m} is the measured permeability of the matrix, cm^2. A 4-MPa overburden pressure was applied to the fractured cores, and the simulated displacement velocity of formation water was 0.3 mL/min. The basic physical parameters of the fractured cores and matrix cores are shown in Table 1.

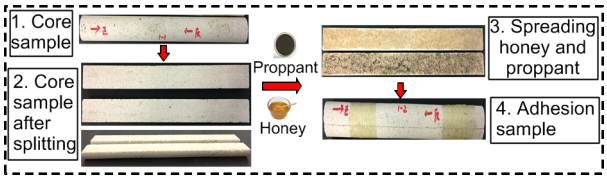

Fig. 3 Process for making fractured carbonate cores

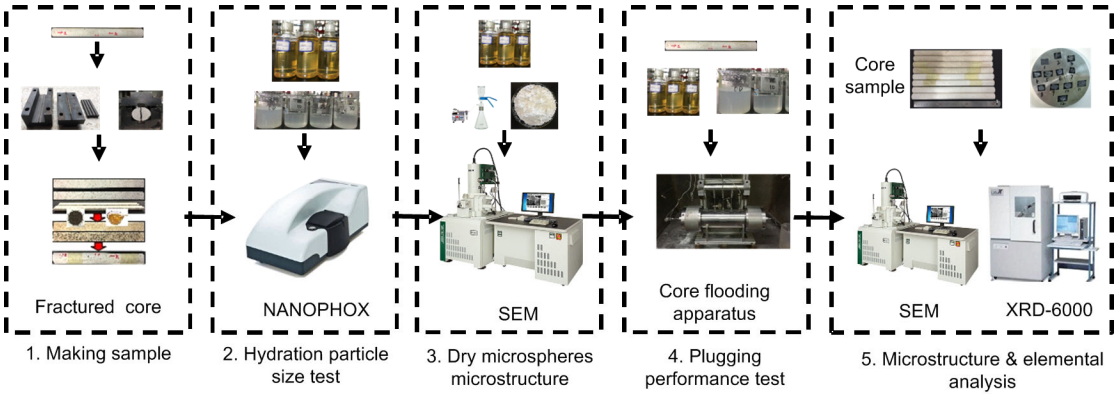

Fig. 2 Experiment flow chart

Table 1 Basic physical parameters of fractured cores and matrix cores

Core No.	Core type	Fluid-measured permeability (mD)	Fracture equivalent width (mm)	Length (cm)	Diameter (cm)	Porosity (%)
1	Matrix core	1.70	–	30.10	2.50	20.71
2	Matrix core	3.60	–	30.10	2.50	21.03
3	Fractured core	43.96	0.0212	30.02	2.49	23.39
4	Fractured core	51.01	0.0227	30.10	2.50	24.48

2.3.3 Demulsification and extraction of PM solution

Because dispersant is organic and will stick around the microspheres, the microscopic morphology of the microspheres before and after expansion cannot be directly observed under the microscope. Therefore, it is necessary to extract the PM from the dispersant to observe the microscopic morphology of the microspheres before and after hydration. A 5-mL polymer microsphere solution was dropped into 100 mL ethanol solution, and the dispersant around the microspheres was thoroughly stirred and washed off. The solution was poured onto filter paper above a funnel, the vacuum filter was turned on, and the ethanol and dispersant were sucked to the bottom, leaving the microspheres on the filter paper. The microspheres on the filter paper were rinsed with pure ethanol 2–3 times, and then the filter paper was removed and dried in an oven for 24 h.

2.3.4 Measurement of microsphere particle size and hydration expansion rate

Since the PM has a strong water control capacity, a low temperature cooling and drying method can effectively reduce the shrinkage of the microspheres during the drying process, and the appearance characteristics of a single PM after hydration expansion can be clearly observed by SEM. The laser nanometer particle size analyzer and SEM were separately used to measure the particle size of polymer microspheres after hydration and observe their microstructure and size after drying for different hydration times. The 0.3% (in weight) polymer microsphere solution was prepared with simulated formation water and placed for 0, 1, 2, or 3 d at 54 °C. Then the particle size of the microspheres was measured and their morphology observed. Three days of hydration was matched with 3 d of shut-in after the completion of site construction, and then production was resumed.

2.3.5 Core flow experiment

Core flow experiments were carried out to evaluate the plugging performance of polymer microspheres on matrix and fractures. The experimental steps were as follows: (1) the core (fractured type/non-fractured type) was put into a core holder with multiple pressure measuring points, and the pressure measuring points, displacement pump, data acquisition system, overburden pump, and other equipment were connected; (2) the polymer microsphere solution, simulated formation water, and kerosene were put in different intermediate containers; (3) the overburden pump was opened and a 4-MPa overburden applied to the core; (4) simulated formation water was injected into the core at 0.3 mL/min to stabilize pressure; the displacement pressure and saturated fluid were recorded to calculate the fluid-measured permeability and porosity; (5) 1.0 PV (pore volume) 0.3% (in weight) polymer microsphere solution was injected into the core at 0.3 mL/min, then the outlet and inlet ends were closed; (6) the oven was opened, and the temperature was set to 54 °C and maintained at that temperature for 3 d to ensure that the microspheres swelled in the core or fracture; (7) the inlet and outlet ends were opened and simulated formation water was forward injected at 0.3 mL/min to stabilize the pressure; (8) the injection end was connected to the outlet end, and the order of the pressure measurement points changed. Kerosene was reversely injected at 0.3 mL/min until the pressure stablized. During the experiment, the displacement pressure and displacement velocity were recorded at each stage to evaluate the injectability and post-expansion plugging performance of microspheres, and the oil/water plugging selectivity. After the experiment, the core was removed for the next experiment. Photographs of the multi-piezometric core flow device are shown in Fig. 4. Fig. 5 is a diagram

showing the distribution of five piezometric points on multi-piezometric core clamp.

2.3.6 Observations of microscopic morphology

SEM imaging and EDS elemental analysis were used to observe the microstructure of polymer microspheres in the core. First, the untested and tested cores were ground, and conductive adhesive was stuck on the loading platform and objective table. Then, the cores were painted on the surface of the conductive adhesive. Each sample coated with rock powder was put into the SEM and EDS elemental analysis equipment to observe the micro-morphology of sealing formed by microspheres in the core, and to analyze the EDS elements on the surface of the rock powder. Results were compared with those from untested rock powder to determine whether the substances adsorbed on the surface of the rock powder belonged to the microspheres.

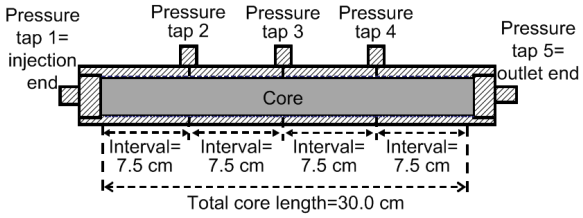

Fig. 5 Schematic diagram of the core gripper

3 Results and discussion

3.1 PM hydration expansion test

Fig. 6a shows the original solution of polymer microspheres, with microspheres uniformly distributed

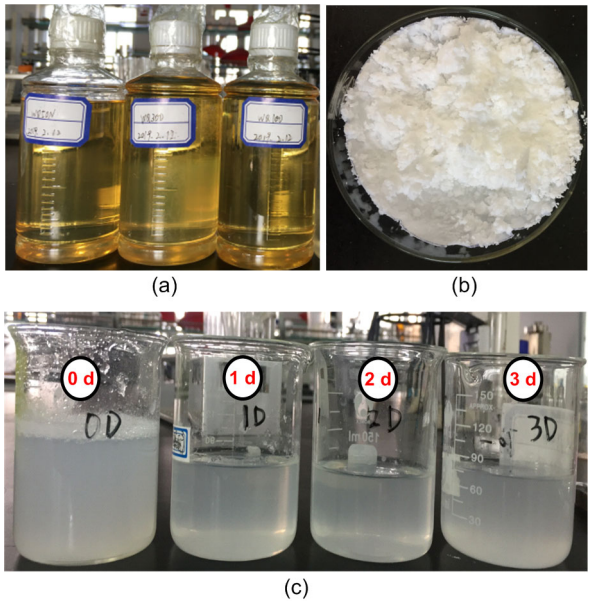

Fig. 6 Original polymer microsphere solution (a), dried pellets after ethanol cleaning and drying (b), and polymer microspheres soaked for different time periods (for particle size testing and SEM micromorphology research) (c)

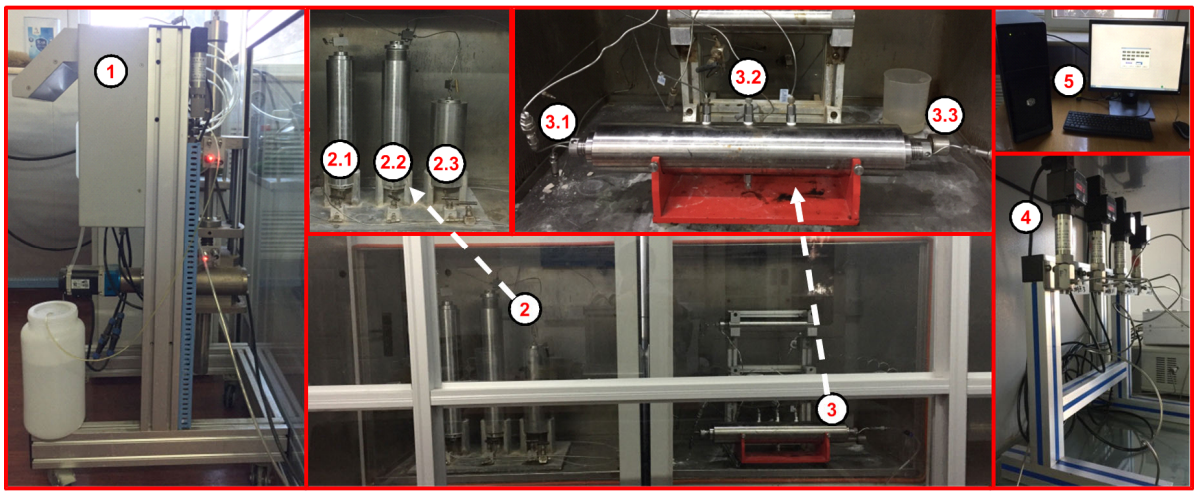

Fig. 4 Photographs of the multi-piezometric core flow device

1: ISCO displacement pump; 2: intermediate vessel (2.1: simulated formation water; 2.2: 0.3% polymer microsphere solution; 2.3: industrial kerosene); 3: multiple pressure point core gripper (3.1: core inlet end; 3.2: pressure point; 3.3: core outlet end); 4: high precision pressure sensor; 5: data acquisition system

in the dispersant. It is transparent and yellowish. Fig. 6b shows the white dried pellet samples obtained after ethanol cleaning and drying.

After hydration for 0, 1, 2, or 3 d at 54 °C (Fig. 6c), the microstructure and size of the microspheres in solution were observed under the SEM after drying. As shown in Fig. 7a, the dried pellets washed with ethanol were observed under the electron microscope to be adsorbed and agglomerated, and the particle size distribution of the monomers ranged from 81.82 to 136.3 nm. Fig. 7b shows the microstructure of the microspheres after 1-d hydration. Since the dispersant had been removed, it can be seen that the microsphere monomer is evenly distributed in the solution. After 1 d of hydration, the particle size distribution of the dry microspheres was between 146.1 and 171.2 nm. Figs. 7c and 7d show the results of hydration for 2 and 3 d, respectively, and the particle size distributions of the microspheres were 302.3–340.9 nm and 413.3–525.8 nm, respectively. The expansion ratio of dry pellets after hydration was calculated (Eq. (2)) to describe the swelling rate of the microspheres (Pu et al., 2018):

$$\mathrm{ER}=\frac{D_2-D_1}{D_1}\times 100\%, \tag{2}$$

where ER is the expansion ratio, and D_1 and D_2 are the diameters of the PM before and after expansion, respectively. The mean particle size measured using the SEM at different hydration times was taken as a reference of microsphere diameter. The reference

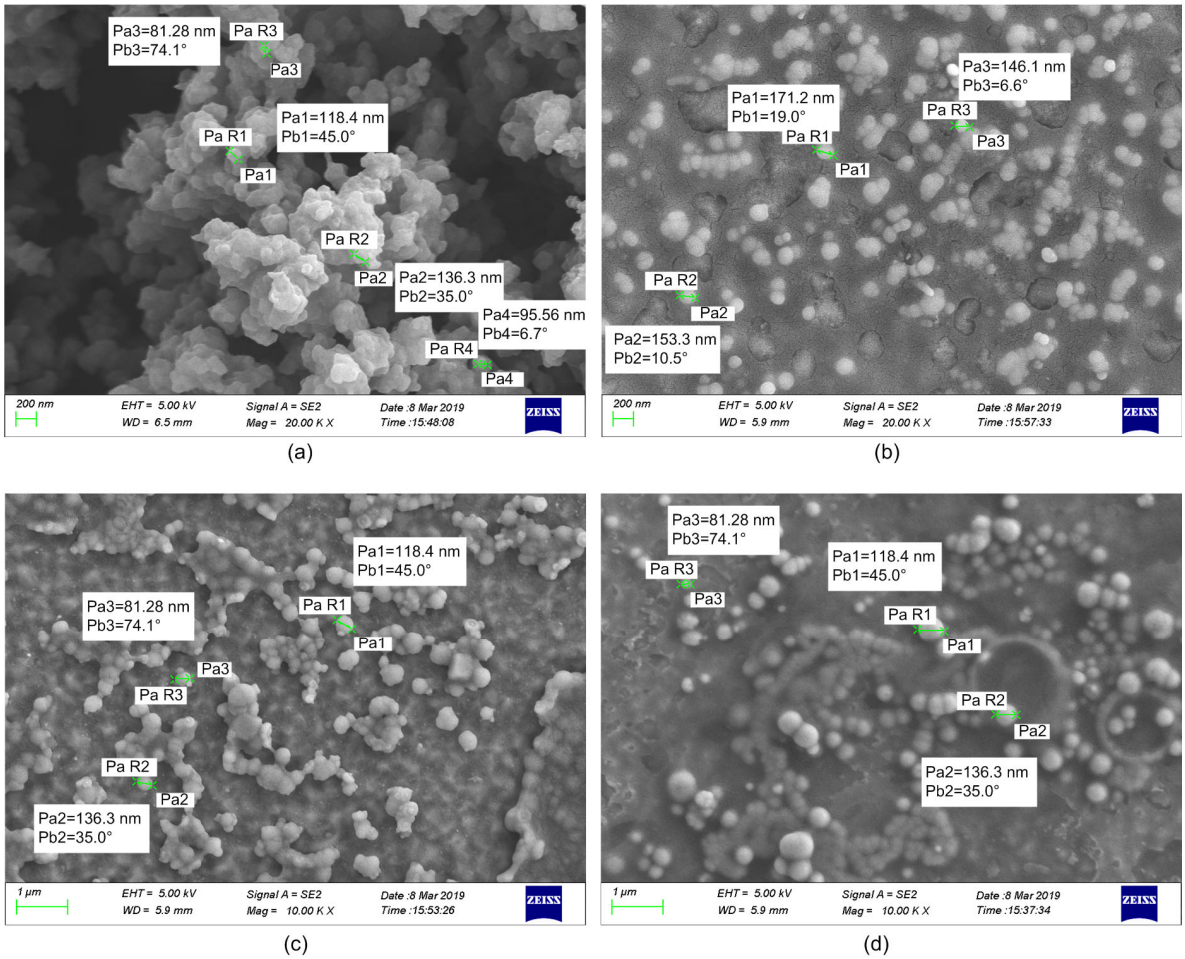

Fig. 7 SEM images showing the morphology and size of polymer microspheres after different hydration times

(a) Microsphere hydration for 0 d (scale: 200 nm); (b) Microsphere hydration for 1 d (scale: 200 nm); (c) Microsphere hydration for 2 d (scale: 1 μm); (d) Microsphere hydration for 3 d (scale: 1 μm). Pa represents the dimension, Pb represents the measurement angle, and Pa R*i* (*i*=1, 2, 3, 4) represents the *i*th measurement point

diameter of the microspheres at 0, 1, 2, and 3 d after hydration was 109.06, 158.65, 321.60, and 469.55 nm, respectively. The corresponding swelling rates were 45.47%, 194.88%, and 330.54% after 1, 2, and 3 d, respectively.

The particle sizes of the polymer microspheres in solution (Fig. 8) were measured using the laser nanoparticle size analyzer shown in Fig. 6c.

The particle sizes of the microspheres in aqueous solution measured at 0–3 d were 125.8, 193.5, 324.3, and 502.4 nm, respectively. The corresponding swelling rates at 1–3 d were 53.82%, 157.79%, and 299.36%, respectively. The expansion rates of microspheres calculated from SEM images and laser particle sizer nanotechnology are plotted together in Fig. 9. The narrow gap between the curves shows the swelling rate of microspheres in solution was close to that of dry microspheres after hydration, particle size was not affected, and the microspheres had good stability both in aqueous solution and in a dry state.

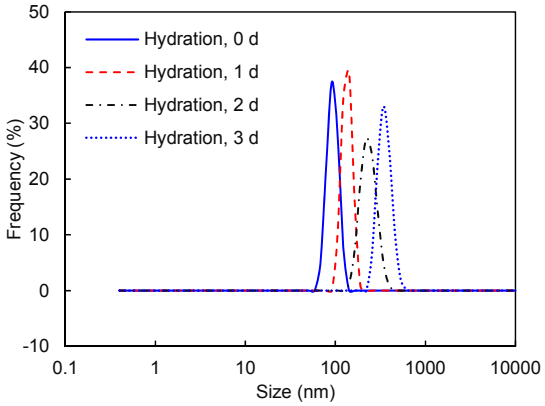

Fig. 8 Particle sizes of microspheres after 0–3 d of hydration

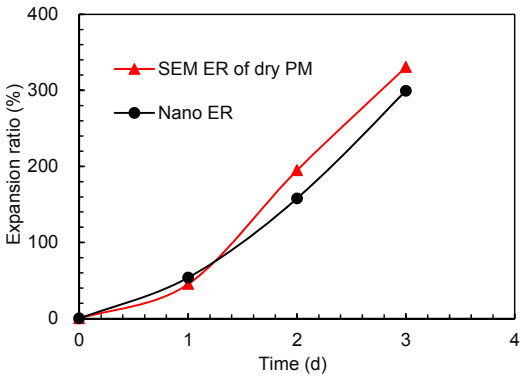

Fig. 9 Calculation results of microsphere expansion ratio

3.2 PM core flow test

The plugging effect of the PM solution in the reservoir was simulated by a core flow experiment. The injection velocity at each stage of the experiment was constantly 0.3 mL/min for the comparison between different stages. The experimental results curve is shown in Fig. 10. According to Figs. 10a–10d, the injection pressure of the PM solution was slightly higher than that of simulated formation water, due mainly to the resistance formed by dispersed microspheres in the solution, which increased the injection pressure of the solution. Although the injection pressure of PM was higher than that of simulated formation water, it still has good injectivity. Good injectivity of PM is the first requirement for realizing a deep plugging effect. To simulate shut-in status after wellsite operation, 1 PV 0.3% (in weight) of PM solution was injected, the equipment was closed, and the oven temperature was set to 54 °C for 3 d. The subsequent water flooding experiment results showed that PM had a certain plugging effect in the core. The subsequent water flooding pressure was higher than the injection pressure of simulated formation water and PM solution before the plugging, and the four pressure measuring points showed a uniform pressure drop, indicating that PM was evenly distributed at the inlet and in the deep core, thereby achieving a deep sealing effect.

The fluid-measured permeability of the core at different stages of formation water injection was compared, and Eqs. (4) and (5) were introduced to calculate the residual resistance coefficient and plugging rate, to quantify the plugging effect of PM. The specific analysis results are described in Section 3.3.

3.3 PM plugging performance evaluation

To study the size matching between the microspheres, core pore throat, and fracture, it is necessary to calculate the size of the core pore throat and fracture. The equivalent sizes of the fracture, obtained in Section 2.3.2, were 0.0212 and 0.0227 mm, respectively. The average pore radius of the core was calculated by (Pu et al., 2018)

$$r = 2 \times \sqrt{\frac{8K}{\Phi}}, \tag{3}$$

where K is the fluid-measured permeability of the core before the experiment, cm^2; r is the average pore radius of the core, cm; Φ is the core porosity. The average pore radii of matrix cores with a permeability of 1.7 mD and 3.6 mD were 0.512 m and 0.740 m, respectively. The concepts of residual drag coefficient R_k and blocking rate η have been introduced (Yue et al., 2007; Zhao et al., 2019). R_k represents the ability of PM to reduce permeability. It is the ratio of the water-phase permeability of the core before and after polymer microsphere plugging, namely the permeability reduction coefficient. η represents the percentage reduction of water phase permeability before and after occlusion by polymer microspheres, reflecting the sealing effect of polymer microspheres:

$$R_k = K_{wb}/K_{wa}, \tag{4}$$

$$\eta = (1 - K_{wa}/K_{wb}) \times 100\%, \tag{5}$$

where K_{wb} and K_{wa} are the water phase permeability of polymer microspheres before and after sealing, respectively, mD. The simulated formation water viscosity was 1 mPa·s at room temperature.

According to Table 2, the residual resistance coefficient of the core matrix and fractured core after

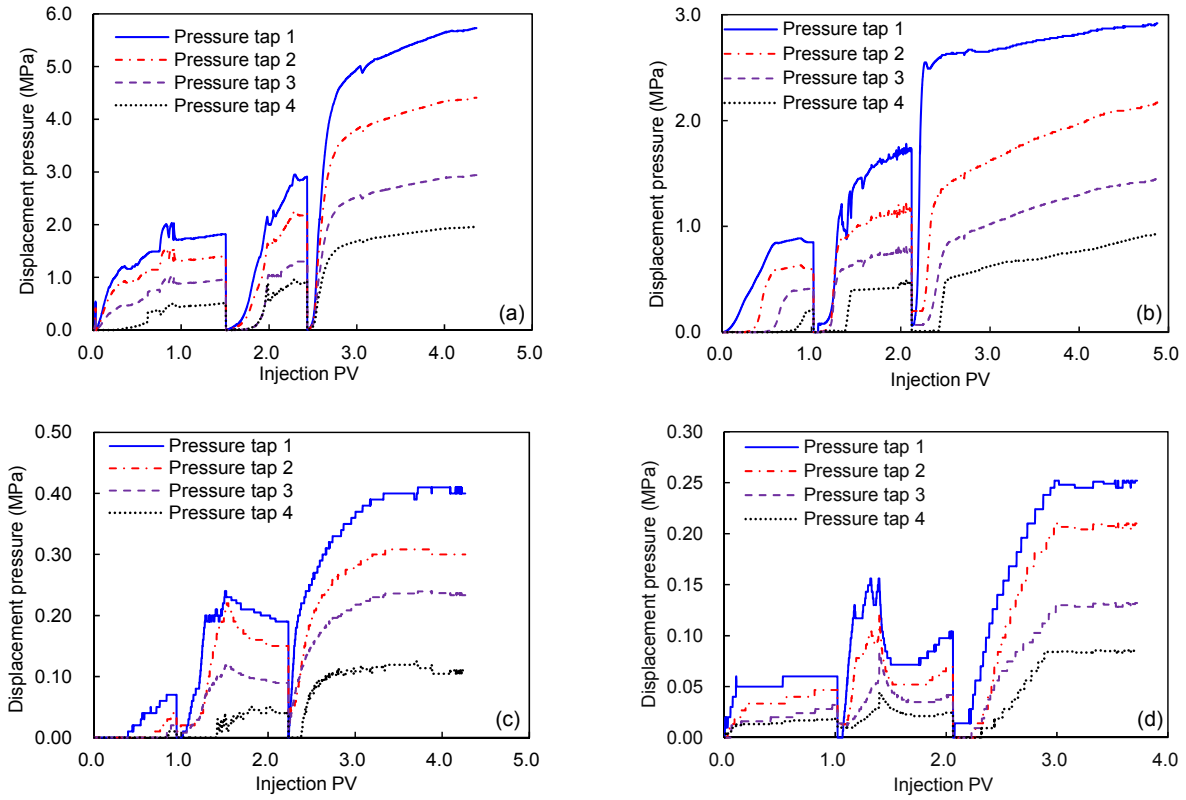

Fig. 10 Plugging curves of the matrix and fractured carbonate cores

(a) 1.70 mD matrix core; (b) 3.60 mD matrix core; (c) 43.96 mD fractured core; (d) 50.01 mD fractured core

Table 2 Physical simulation results of PM plugging performance

Initial particle size of microsphere (nm)	Core type	Water flood permeability before plugging (mD)	Porosity (%)	Hole throat or fracture diameter (μm)	Water flood permeability after plugging (mD)	Residual resistance coefficient	Sealing rate (%)
125.8	Matrix core	1.70	20.71	0.512	0.52	3.29	69.58
	Matrix core	3.60	21.03	0.740	1.05	3.42	70.79
	Fractured	43.96	23.39	21.20	7.47	5.88	83.01
	Fractured	50.01	24.48	22.70	12.24	4.17	76.00

plugging was between 3.29 and 5.88, and the plugging rate between 69.58% and 83.01%. The higher the residual resistance coefficient, the higher the plugging rate. Effective plugging formed after the hydration expansion of the PM, and the average plugging rate was over 70%.

3.4 PM oil/water selective plugging performance

Water plugging by PM is the key to the success of reducing water production without affecting oil production. After the completion of subsequent water flooding, the core injection end and the outlet end were swapped during the simulated reservoir oil production process, and kerosene was injected reversely at a rate of 0.3 mL/min. The experimental results curves are shown in Figs. 11a–11d. The forward formation water injection pressures after 1.70, 3.60, 43.96, and 50.01 mD core plugging were 5.95, 2.91, 0.41, and 0.25 MPa, respectively, while the reverse kerosene injection pressures were 2.46, 1.89, 0.22, and 0.084 MPa, respectively. Eq. (6) is introduced to calculate the PM oil/water selectivity ratio:

$$R_{w/o} = K_{wa} / K_{oa}, \tag{6}$$

where $R_{w/o}$ is the oil/water selectivity coefficient; K_{wa} is the positive water-phase permeability after PM plugging, mD; K_{oa} is the reverse oil-phase permeability after PM sealing, mD. When $R_{w/o}$=1, the PM had a considerable sealing effect on simulated formation water and kerosene, and was not selective; when $0<R_{w/o}<1$, the PM had a certain selectivity of oil/water, blocking water but not oil, and the smaller $R_{w/o}$ the better the sealing selectivity. When $R_{w/o}>1$, the sealing effect of PM on kerosene was higher than that of simulated formation water, which was not conducive to the application of well water plugging. Kerosene viscosity was 2 mPa·s at 54 °C.

Table 3 shows the calculated PM selective plugging coefficients. The PM had a strong oil/water

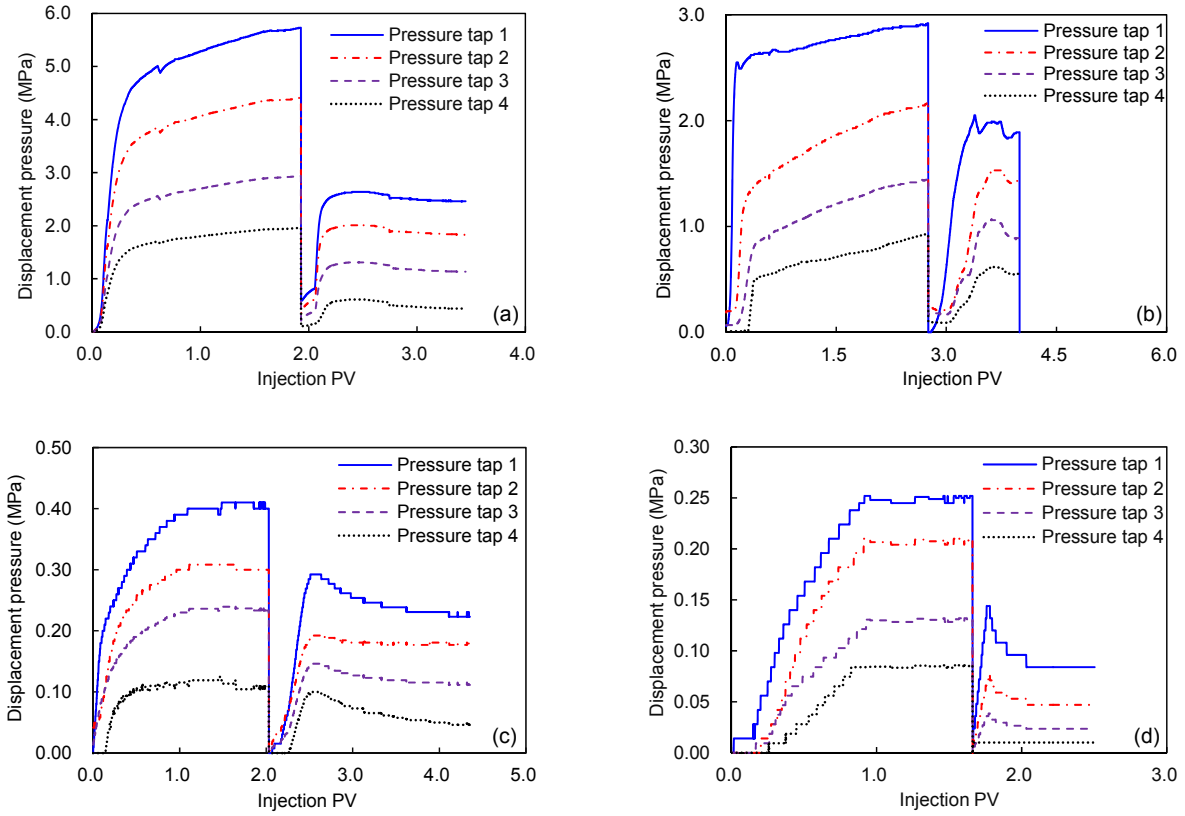

Fig. 11 Curves of experimental results for oil/water selective plugging of matrix and fractured carbonate core
(a) 1.70 mD matrix core; (b) 3.60 mD matrix core; (c) 43.96 mD fractured core; (d) 50.01 mD fractured core

selective plugging effect when the selection coefficient $R_{w/o}$ was less than 1.0 and close to 0. According to Figs. 11a–11d, the pressure drop of oil/water selective plugging was even in the sections, achieving the effect of even and selective blocking across sections. The main reason for PM oil/water selective water plugging is that oil/water and PM have different working mechanisms. When PM meets water it will swell, the surface viscosity will increase, and it will stick to the carbonate rock wall. Different microspheres will agglomerate to form larger particles, increasing the plugging effect against injected water. PM particles are insoluble in most organic solvents, and the performance of PM in kerosene is stable and does not produce swelling and adhesion effects. Therefore, there was a low plugging effect on reverse injection of kerosene, reflecting the oil/water selective plugging function of PM (Dawe and Zhang, 1994; Liang et al., 1995; Yang et al., 2012). Fig. 12 is a schematic diagram of the oil/water selective plugging mechanism.

3.5 Interior changes in core before and after PM plugging

To study the microscopic mechanism of PM in the core throat and fractures before and after sealing, SEM imaging was performed on the cores used in the experiment (Figs. 13 and 14). Zoom to 2 μm, showed that a large number of polymer microsphere particles were adsorbed on the surface of the rock particles after PM injection, and the particles were adsorbed as monomers or aggregates. Zoom to 200 nm showed that PM agglomerated and had gel-like material on the surface, which reduced the roughness of the surface of the rock particles and the size of the core throat. A colloidal substance produces strong resistance when it meets water and produces a low sealing effect when it meets oil.

Therefore, the plugging mechanism of PM in the core throat or a natural microfracture includes three main aspects: (1) PM monomer adsorbs on the surface of rock particles, reducing the size of the throat, and many single particles increase the specific surface area of the inner layer, reducing the permeability; (2)

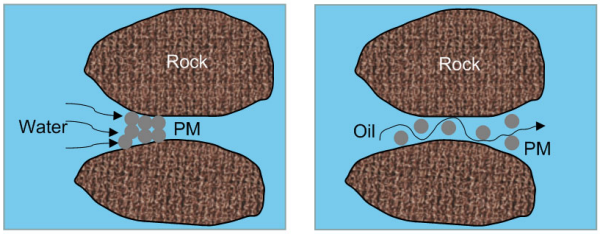

Fig. 12 Schematic diagram of the oil/water selective plugging mechanism

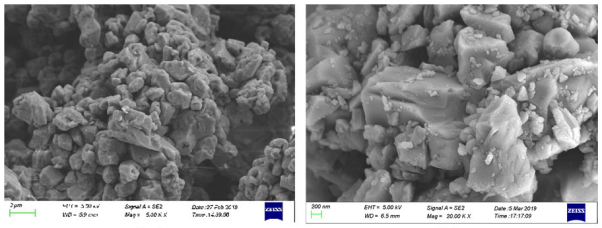

Fig. 13 SEM images of clean carbonate rock powder
(a) Scale bar of 2 μm; (b) Scale bar of 200 nm

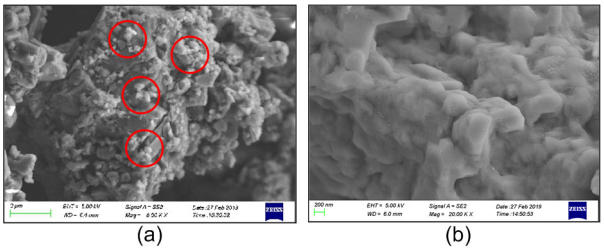

Fig. 14 SEM images of carbonate rock powder after the plugging experiment
(a) Scale bar of 2 μm; (b) Scale bar of 200 nm

Table 3 Calculated plugging selection coefficients of PM

Initial particle size of microsphere (nm)	Core type	Water flood permeability after plugging (mD)	Porosity (%)	Pore throat or fracture diameter (μm)	Reverse oil driving permeability after plugging (mD)	Oil/Water selectivity coefficient
125.8	Matrix core	0.52	20.71	0.512	2.50	0.21
	Matrix core	1.05	21.03	0.740	3.24	0.32
	Fractured	7.47	23.39	21.20	27.82	0.27
	Fractured	12.24	24.48	22.70	73.27	0.17

mechanical trapping occurs in the small-sized pores after the PM swells; (3) numerous PM monomer particles are agglomerated into a network structure to block large pores. Fig. 15 is a schematic diagram of the plugging mechanism of PM in the core.

To further verify whether the substances adsorbed on the surface of the rock particles were PM, the components of the clean rock particles, the rock particles after the plugging experiment, and the PM powder were analyzed by EDS elemental analysis.

The results are shown in Figs. 16–18. The main components of clean rock particles were 32.33% (in weight) Ca, 56.38% O, and 9.07% C. After the plugging experiment, the content of C on the surface of the rock particles was as high as 47.78%, which is close to the content of the main component C of PM (61.95%), indicating that the main component of the rock particle surface adsorption after the plugging experiment was PM. The EDS results in Fig. 17 show the absence of calcium, due mainly to the adsorption of nanospheres on the core surface, which hindered the EDS scan results.

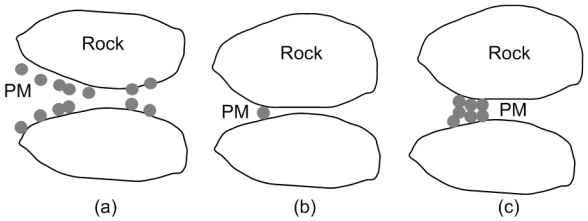

Fig. 15 Schematic diagram of the PM plugging mechanism in the core

(a) Adsorption retention; (b) Mechanical capture in a small hole; (c) Agglomeration blocks in a large hole

Element	C K	O K	Na K	Mg K	Al K	Si K	Cl K	K K	Ca K
Weight (%)	9.07	56.38	0.72	0.27	0.36	0.21	0.47	0.19	32.33
Atomic (%)	14.62	68.20	0.61	0.21	0.26	0.15	0.25	0.09	15.61

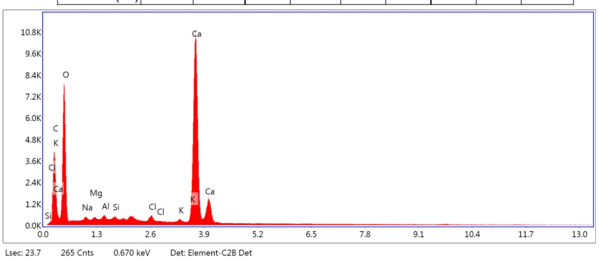

Fig. 16 EDS elemental analysis results of clean rock particles

Element	C K	O K	Na K	K K
Weight (%)	47.78	34.96	17.17	0.10
Atomic (%)	57.55	31.61	10.80	0.04

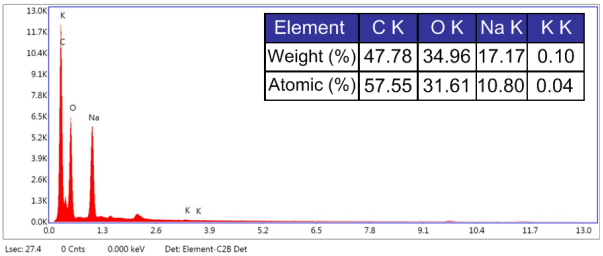

Fig. 17 Analysis results of rock particle EDS elements after the plugging experiment

Element	C K	O K	Na K	Al K	S K
Weight (%)	61.95	30.33	4.21	0.23	3.29
Atomic (%)	70.20	25.80	2.49	0.11	1.40

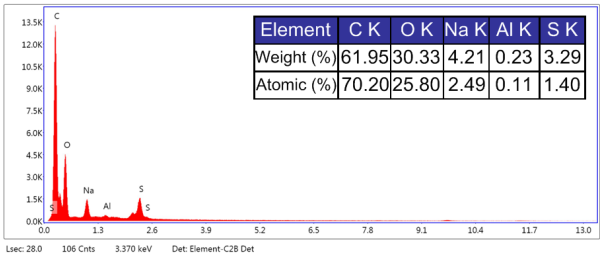

Fig. 18 EDS element analysis results of PM powder

4 Conclusions

In this study of nanoscale PM solution, cores from a fractured carbonate reservoir in the Troyes oilfield in north Kazakhstan, with a reservoir temperature of 54 °C and a natural fracture size of 0.02–0.03 mm, were chosen for model making. A comprehensive evaluation of the sealing effect and oil/water selectivity of PM in carbonate matrix cores and fractured cores was conducted using a PM basic performance test, core flow experiment, and micro means of SEM and EDS. The main conclusions were as follows:

1. PM has good dispersibility and swelling ability in water; the swelling rate after 3 d reached over 300%. PM also has a strong tolerance to high salinity brine.

2. PM has a good deep plugging effect in both a matrix core and a fractured core. The 30 cm-long core model plugging experiment showed that the segmental pressure drop after plugging was evenly distributed. The residual resistance coefficient of sealed matrix core and fractured core was between 3.29 and 5.88, the blocking rate was between 69.58% and 83.01%, and the larger the residual resistance coefficient, the higher the blocking rate. The average

blocking rate of PM after hydration and expansion in the core was as high as 70% or more.

3. The oil/water selection coefficient $R_{w/o}$ of PM plugging was less than 1.0 and close to 0. PM has a strong oil/water selective plugging effect. The main reason is the different functional mechanisms of oil/water and PM; PM swells after hydration, the surface viscosity increases, and the PM adheres to the wall of carbonate rock. Different microspheres agglomerate to form larger volume particles, increasing the sealing of injected water. PM has stable performance in kerosene without causing a swelling and blocking effect, so it has a lower sealing effect on reverse injection of kerosene.

4. The results of SEM imaging analysis suggest that the plugging mechanism of PM in the core throat or natural micro-fracture includes three main aspects: (1) PM monomer adsorbs on the surface of rock particles, reducing the size of the throat, while many single particles increase the intra-layer specific surface area of inner layer and reduce the permeability; (2) Mechanical trapping occurs in the small-sized pores after the PM swells; (3) Numerous PM monomer particles agglomerate into a network structure to block large pores. EDS elemental analysis technology validated the functional mechanism.

Contributors

Conceptualization, Jie WANG and Fu-jian ZHOU; methodology, Jun-jian LI; formal analysis and validation, Kai YANG and Lu-feng ZHANG; funding acquisition, Fu-jian ZHOU; writing of original draft, Jie WANG and Fan FAN; review and editing, Fu-jian ZHOU.

Conflict of interest

Jie WANG, Fu-jian ZHOU, Jun-jian LI, Kai YANG, Lu-feng ZHANG, and Fan FAN declare that they have no conflict of interest.

References

Al-Anazi HA, Sharma MM, 2002. Use of a pH sensitive polymer for conformance control. Proceedings of the International Symposium and Exhibition on Formation Damage Control, SPE-73782-MS. https://doi.org/10.2118/73782-MS

Al-Ibadi A, Civan F, 2012. Experimental study of gel particles transport through porous media. Proceedings of the SPE Latin America and Caribbean Petroleum Engineering Conference, SPE-153557-MS. https://doi.org/10.2118/153557-MS

Al-Ibadi A, Civan F, 2013. Experimental investigation and correlation of thermal effects on near-wellbore formation treatment by gel particles. Proceedings of the SPE International Symposium on Oilfield Chemistry, SPE-164119-MS. https://doi.org/10.2118/164119-MS

Bai BJ, Wei MZ, Liu YZ, 2013. Field and lab experience with a successful preformed particle gel conformance control technology. Proceedings of the SPE Production and Operations Symposium, SPE-164511-MS. https://doi.org/10.2118/164511-MS

Dawe RA, Zhang YP, 1994. Mechanistic study of the selective action of oil and water penetrating into a gel emplaced in a porous medium. *Journal of Petroleum Science and Engineering*, 12(2):113-125. https://doi.org/10.1016/0920-4105(94)90011-6

Dong ZX, Li YH, Lin MQ, et al., 2009. Rheological properties of polymer micro-gel dispersions. *Petroleum Science*, 6(3):294-298. https://doi.org/10.1007/s12182-009-0047-3

Frampton H, Morgan JC, Cheung SK, et al., 2004. Development of a novel waterflood conformance control system. Proceedings of the SPE/DOE Symposium on Improved Oil Recovery, SPE-89391-MS. https://doi.org/10.2118/89391-MS

Hua Z, Lin MQ, Dong ZX, et al., 2014. Study of deep profile control and oil displacement technologies with nanoscale polymer microspheres. *Journal of Colloid and Interface Science*, 424:67-74. https://doi.org/10.1016/j.jcis.2014.03.019

Liang JT, Sun HW, Seright RS, 1995. Why do gels reduce water permeability more than oil permeability? *SPE Reservoir Engineering*, 10(4):282-286. https://doi.org/10.2118/27829-PA

Pu WF, Zhao S, Wang S, et al., 2018. Investigation into the migration of polymer microspheres (PMs) in porous media: implications for profile control and oil displacement. *Colloids and Surfaces A: Physicochemical and Engineering Aspects*, 540:265-275. https://doi.org/10.1016/j.colsurfa.2018.01.018

Ranganathan R, Lewis R, Mccool CS, et al., 1998. Experimental study of the gelation behavior of a polyacrylamide/aluminum citrate colloidal-dispersion gel system. *SPE Journal*, 3(4):337-343. https://doi.org/10.2118/52503-PA

Rousseau D, Chauveteau G, Renard M, et al., 2005. Rheology and transport in porous media of new water shutoff/conformance control microgels. Proceedings of the SPE International Symposium on Oilfield Chemistry, SPE-93254-MS. https://doi.org/10.2118/1105-0071-JPT

Wu YS, Bai BJ, 2008. Modeling particle gel propagation in porous media. Proceedings of the SPE Annual Technical Conference and Exhibition, SPE-115678-MS. https://doi.org/10.2118/115678-MS

Yang S, Wei J, 2015. Reservoir Physics. Schlumberger, Houston, USA, p.152-155.

Yang Y, Wang YF, Zhang P, et al., 2012. Mechanisms and influencing factors of selective water shutoff agents. *Oilfield Chemistry*, 29(4):502-506 (in Chinese). https://doi.org/10.19346/j.cnki.1000-4092.2012.04.027

Yao CJ, Xu XH, Wang D, et al., 2016. Research and application of micron-size polyacrylamide elastic microspheres (MPEMs) as a smart sweep improvement and profile modification agent. Proceedings of the SPE Improved Oil Recovery Conference, SPE-179531-MS. https://doi.org/10.2118/179531-MS

Yue XA, Wang YF, Wang KL, 2007. Improve Oil Recovery Basis. Petroleum Industry Publishing House, Beijing, China, p.92-93 (in Chinese).

Zhao S, Pu WF, Wei B, et al., 2019. A comprehensive investigation of polymer microspheres (PMs) migration in porous media: EOR implication. *Fuel*, 235:249-258. https://doi.org/10.1016/j.fuel.2018.07.125

中文概要

题　目：纳米聚合物微球在裂缝型碳酸盐岩储层油/水选择性封堵性能评价

目　的：对聚合物微球（PM）在碳酸盐岩基质岩心与裂缝型岩心中封堵效果和油/水选择性进行综合评价。

创新点：1. 制作裂缝型碳酸盐岩模型并进行等效缝宽度计算；2. 显微评价 PM 的水化膨胀特性；3. 进行聚合物微球深层封堵性能评价；4. 进行聚合物微球油/水选择性封堵评估。

方　法：采用纳米级聚合物微球溶液，并以哈萨克斯坦北特鲁瓦裂缝型碳酸盐岩油藏储层温度（54 ℃）和碳酸盐岩天然裂缝尺寸（0.02~0.03 mm）为实验条件；通过碳酸盐岩裂缝型岩心模型制作、PM 基本性能测试、岩心流动实验以及扫描式电子显微镜（SEM）和能谱分析仪（EDS）等微观手段，对 PM 在碳酸盐岩基质岩心与裂缝型岩心中封堵效果和油/水选择性进行综合评价。

结　论：1. PM 在水中具有良好的分散性和溶胀能力，3 d 溶胀率高达 300%以上，且对高矿化度盐水具有较强的耐受性。2. PM 在基质岩心和裂缝型岩心均具有较好的深部封堵效果；30 cm 长岩心模型封堵实验表明，封堵后的分段压降均匀分布，岩心基质和裂缝型岩心封堵后的残余阻力系数介于 3.29~5.88，封堵率介于 69.58%~83.01%，且残余阻力系数越大，封堵率越高；PM 在岩心中水化膨胀后可形成有效封堵，且平均封堵率高达 70%以上。3. PM 封堵的油/水选择系数 $R_{w/o}$ 均小于 1.0 且接近于 0，说明 PM 具有较强的油/水选择性封堵效果；这主要是因为油/水与 PM 作用机理不同；PM 遇水后溶胀且表面粘性增加而粘连在碳酸盐岩壁面，并且不同微球之间相互团聚形成较大体积的颗粒，因此增加了对注入水的封堵效果；PM 在煤油中则性能稳定，不产生溶胀和粘连效果，因此对反向注入煤油具有较低的封堵效果。4. SEM 成像结果分析认为，PM 在岩心喉道或天然微裂缝中的封堵机理主要包括三个方面：（1）PM 单体在岩石颗粒表面吸附，降低喉道的尺寸，同时多个单颗粒小球增大了层内比表面积、降低了层内渗透率；（2）PM 溶胀后在小尺寸孔道形成了机械捕集；（3）多个 PM 单体颗粒团聚成网状结构堵塞了大孔道。EDS 元素分析技术进一步验证了其作用机理。

关键词：纳米聚合物微球；裂缝型岩心；封堵率；油/水选择性；封堵机理